Experimental determination of the ^{36}Cl$(n,p)^{36}$S and ^{36}Cl$(n,\alpha)^{33}$P reaction cross sections and the consequences on the origin of ^{36}S

L. De Smet,* C. Wagemans,† and G. Goeminne‡
Department of Subatomic and Radiation Physics, University of Gent, Proeftuinstraat 86, B-9000 Gent, Belgium

J. Heyse§ and J. Van Gils
Institute for Reference Materials and Measurements, EC-JRC, Retieseweg 111, B-2440 Geel, Belgium

(Received 20 December 2006; published 28 March 2007)

The ^{36}Cl$(n,p)^{36}$S and ^{36}Cl$(n,\alpha)^{33}$P reaction cross sections have been studied with resonance neutrons at the linear accelerator GELINA of the IRMM in Geel (Belgium) and have been determined up to approximately 250 keV using the time-of-flight technique. In this energy region, 17 resonances were observed, whereas eight were identified before. For some resonances the resonance strength, the spin, and the total width could be determined. From the obtained cross section data, the MACS has been calculated by numerical integration. These updated MACS values were used in stellar models to trace the origin of the rare isotope ^{36}S.

DOI: 10.1103/PhysRevC.75.034617 PACS number(s): 25.40.Fq, 27.30.+t, 97.10.Cv

I. INTRODUCTION

Up to now, only two measurements of the energy dependence of the ^{36}Cl$(n,p)^{36}$S and ^{36}Cl$(n,\alpha)^{33}$P cross sections were performed. Gledenov *et al.* [1] observed three resonances up to 10 keV and Koehler *et al.* [2] identified eight resonances in the energy region between 900 eV and 70 keV. However, both measurements suffered from a poor energy resolution. Therefore, a new series of measurements of the energy dependence at the GELINA facility of the Institute for Reference Materials and Measurements (IRMM) in Geel (Belgium) was performed. Partial or preliminary results have already been reported [3–5].

Apart from the obtained cross section values, the measurements provide interesting nuclear physics information: the energy position, strength, spin, and total level width for some of the states in the formed compound nucleus could be determined.

Neutron induced reactions on ^{36}Cl ($T_{1/2} = 3.0 \times 10^5$ y) are important in the quest for the origin of the rare neutron rich isotope ^{36}S. Its formation cannot be attributed to thermonuclear fusion reactions, which is the case for most of the elements up to iron. An alternative mechanism for the production of the major part of ^{36}S would be the weak component of the s-process in massive stars. To verify this hypothesis nucleosynthesis network calculations are necessary, requiring accurate cross section data for the reactions involved. As the ^{36}Cl$(n,p)^{36}$S reaction immediately leads to ^{36}S, it influences the ^{36}S abundance in a direct way. On the other hand, ^{36}Cl$(n,\alpha)^{33}$P causes a recycling to ^{33}P, which undergoes β^--decay to ^{33}S which can still form ^{36}S through successive n-captures. The updated Maxwellian averaged cross section (MACS) values obtained in the present work are used in stellar model calculations and the influence on the ^{36}S production is discussed.

II. EXPERIMENTAL SETUP AND DATA REDUCTION

A. Experimental setup

The ^{36}Cl$(n,p)^{36}$S and ^{36}Cl$(n,\alpha)^{33}$P reactions were performed at a 30.39 m long flight path of the GELINA neutron time-of-flight facility. The linac produces a pulsed electron beam. The high-energy electrons hit a cooled and rotating uranium target, in which they are slowed down and generate Bremsstrahlung γ-rays. The neutrons are then produced via (γ,n) and (γ,f) reactions. To increase the number of slow neutrons, two water-filled beryllium moderators are placed above and below the uranium target. The resulting neutron energy distribution can be characterized by a Maxwellian distribution at thermal energy and a high energy tail with approximately a 1/E-shape. The neutron energy spectrum ranges from a few meV up to a few MeV. The time-of-flight method (TOF) is applied to determine the energy of the interacting neutrons. More detailed information about the GELINA facility can be found in [6,7].

For the detection of the protons and α-particles, a Frisch gridded ionization chamber filled with ultra pure methane as detector gas was used [8]. The settings of the ionization chamber (gas pressure, electrode distances, and electric fields) were adjusted to detect protons and α-particles. The level scheme from Fig. 1 shows the possible transitions and the corresponding particle energies are listed in Table I. The signals from the anode and cathode are amplified and sent to an analog-to-digital converter (ADC). A third signal is sent from the amplifier on the cathode side to a timing single channel analyser (TSCA). If this signal lies between some predefined levels, a fast logic signal T_n is sent to a time coder (TC) and serves as a stop signal. The start signal T_0 is generated by the linear accelerator and is sent to the time coder just before the

*Electronic address: liesbeth.desmet@gmail.com
†Electronic address: cyrillus.wagemans@UGent.be
‡Present address: Centre for Sustainable Development, University of Gent, Poel 16, B-9000 Gent, Belgium.
§Present address: SCK•CEN, Boeretang 200, B-2400 Mol, Belgium.

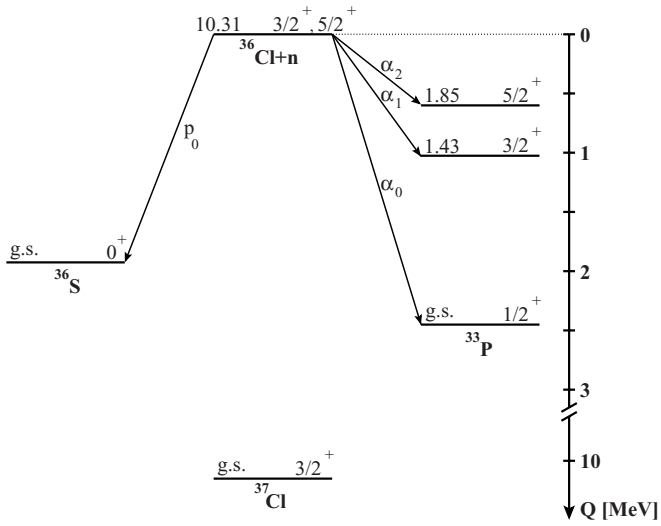

FIG. 1. Level scheme for the ^{36}Cl$(n,p)^{36}$S and ^{36}Cl$(n,\alpha_i)^{33}$P reactions.

electrons impinge on the uranium target. The TC calculates the time difference between T_n and T_0 for each event and converts it into a TOF channel number. At this point both ADC and TOF channel numbers are handled by the LABVIEW-based data acquisition system 2000-DAQ developed at the IRMM [9] and are stored on a PC for offline analysis.

For all the measurements, the accelerator was operated at a repetition frequency of 800 Hz and the electron bursts had a width of 1 ns. To remove neutrons from previous bursts, a boron overlap filter was permanently placed in the neutron beam. The time dependent background was determined in a separate measurement by putting black resonance filters such as Au, Co, Mn, Rh, and W in the neutron beam.

The ^{36}Cl sample was prepared at the IRMM by vacuum deposition of silver chloride on an aluminium foil, which ensures the homogeneity of the layer. The effective area of the silver chloride deposit was 6×5 cm^2. The sample had a ^{36}Cl enrichment of 40.50%, the other isotopes being ^{35}Cl and ^{37}Cl. To avoid chemical reactions of the silver chloride with the aluminium foil, the latter was covered with a platinum coating. The more common chemical forms sodium or potassium chloride were not used because they are more hygroscopic. To determine the number of ^{36}Cl atoms (N_{Cl}), the sample was irradiated with thermal neutrons at the High Flux Reactor of the ILL (France). From the proton count rate (Y_p) of the measured ^{36}Cl$(n_{\mathrm{th}},p)^{36}$S reaction [10], the number of ^{36}Cl atoms could be calculated from

$$Y_p = \sigma_{36} N_{Cl} \varphi_n, \tag{1}$$

with φ_n the neutron flux from the reactor, which was determined via the well-known thermal neutron induced fission cross section of ^{235}U, and σ_{36} the known cross section of the ^{36}Cl$(n_{\mathrm{th}},p)^{36}$S reaction. The sample used in this measurement contained $(1.39 \pm 0.07) \times 10^{19}$ ^{36}Cl atoms. More details about the preparation and thickness determination of the ^{36}Cl sample can be found in [11].

For the neutron flux determination, an evaporated elemental ^{10}B layer was used, containing $(7.17 \pm 0.13) \times 10^{19}$ atoms.

TABLE I. Q-values and corresponding energies for the possible ^{36}Cl$(n,p)^{36}$S and ^{36}Cl$(n,\alpha_i)^{33}$P reactions.

	Q-value [MeV]	E [MeV]
p_0	1.924	1.872
α_0	2.462	2.196
α_1	1.030	0.919
α_2	0.614	0.548

B. Data reduction

The total observed count rate $Y_{\mathrm{Cl}}(E_n)$ for a neutron induced reaction as a function of the neutron energy is

$$Y_{\mathrm{Cl}}(E_n) = \epsilon_{\mathrm{Cl}} N_{\mathrm{Cl}} \sigma_{\mathrm{Cl}}(E_n) \varphi(E_n) + Y_{\mathrm{Cl}}^{BG}(E_n), \tag{2}$$

where ϵ_{Cl} is the detector efficiency and N_{Cl} the number of atoms in the ^{36}Cl sample used. $\sigma_{\mathrm{Cl}}(E_n)$ is the differential neutron induced cross section to be determined and $\varphi(E_n)$ represents the neutron flux. The neutron flux is determined by detecting the ^{10}B$(n,\alpha)^7$Li reaction products during a separate measurement. An identical relation for the flux count rate can be adopted:

$$Y_B(E_n) = \epsilon_B N_B \sigma_B(E_n) \varphi(E_n) + Y_B^{BG}(E_n). \tag{3}$$

In this case the $\sigma_B(E_n)$ cross section is known and is taken from the ENDF/B-VI database [12]. In both cases the time dependent background $Y^{BG}(\mathrm{TOF})$ – which is equivalent to the energy dependent background $Y^{BG}(E_n)$ – has been determined by fitting a function $Y^{BG}(\mathrm{TOF}) = a \cdot \mathrm{TOF}^b + c$ through the count rates in the black resonance regions and has been subtracted from the count rates $Y_{\mathrm{Cl}}(\mathrm{TOF})$ and $Y_B(\mathrm{TOF})$. By dividing relation (2) and (3), the differential neutron induced cross section of ^{36}Cl can be calculated as follows:

$$\sigma_{\mathrm{Cl}}(E_n) = \frac{\epsilon_B}{\epsilon_{\mathrm{Cl}}} \frac{Y_{\mathrm{Cl}}(E_n) - Y_{\mathrm{Cl}}^{BG}(E_n)}{Y_B(E_n) - Y_B^{BG}(E_n)} \frac{N_B}{N_{\mathrm{Cl}}} \sigma_B(E_n). \tag{4}$$

The ^{36}Cl(n,p), ^{36}Cl(n,α) as well as the ^{10}B(n,α) reactions have been determined in the same experimental conditions, so $\frac{\epsilon_B}{\epsilon_{Cl}} = 1$ (detection geometry is 2π). However, for higher neutron energies (>10 keV) both reaction products from the ^{10}B$(n,\alpha)^7$Li reaction were not always detected as a result of the influence of the center of mass velocity which might not be neglected for light mass nuclei. It has been verified that this is not the case for the ^{36}Cl(n,p) or ^{36}Cl(n,α) reactions. Therefore this small anisotropy has been taken into account only for the ^{10}B(n,α) reaction and after subtracting the background contribution from the flux count rate.

From the level scheme in figure 1 it can be seen that the energy of the detected protons and α_0-particles is 1.9 MeV and 2.2 MeV, respectively. The α_1- and α_2-transitions are allowed, but as these particles have low energies, their probability to penetrate the Coulomb barrier is very small. These transitions were not observed in this experiment. This was neither the case in the thermal measurement performed by Wagemans *et al.* [10] at the ILL in Grenoble. As the energy difference

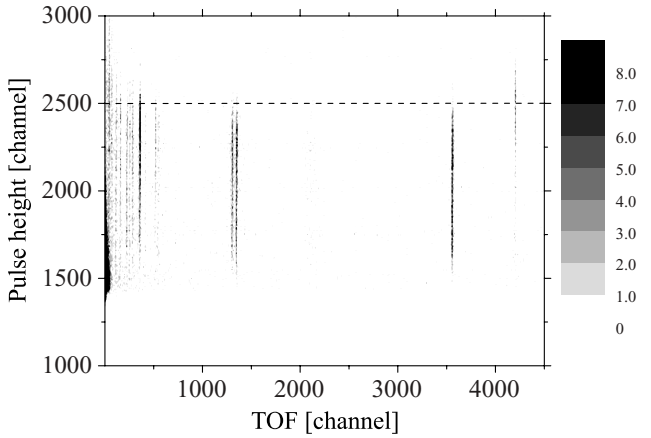

FIG. 2. Cathode versus TOF spectrum after putting appropriate software windows on anode and cathode pulse heights. The dashed line illustrates that only the first resonance at highest TOF (∼channel 4250) has a significant α-contribution, as the other resonances have no counts above this line.

between the protons and α_0-particles is low, it was not easy to make a good separation in the pulse height spectrum. The pulse height versus time-of-flight spectrum for the $(n,p)+(n,\alpha)$ measurement is shown in Fig. 2. It illustrates that only the lowest energy resonance at TOF $\sim$ 4250 has a significant α-contribution, as only this resonance has a significant amount of counts in the pulse height spectrum above channel number 2500 (dotted line), which corresponds to the upper limit for 1.872 MeV proton detection. In the TOF region below channel number 500, some counts appear above the dotted line. This is mainly due to the kinetic energy of the inducing neutrons which has to be taken into account in this energy region. It leads to a slightly higher energy for the emitted particles than tabulated before, which results in counts appearing at higher pulse height channels. The width of the pulse height distribution is proportional to the range of the charged particles in the ionizing gas. In our setup this range is roughly six times larger for the protons than for the α-particles, leading to a broader proton distribution in the pulse height spectrum. Eventually, by comparing the pulse height spectrum of the first resonance with the spectra for the other resonances, an α-contribution of $(76 \pm 7)\%$ has been estimated in the first resonance. All the other resonances do not show an enhancement at higher pulse heights, therefore they are regarded as proton resonances with a negligible α-contribution. This result is in agreement with the experiment performed by Koehler *et al.* [2]. They found that $(n,\alpha)/(n,p) = 3.0$ for the first resonance and for the other resonances the (n,α)-contribution appeared to be very small.

Because of the difficulty in making a perfect separation between protons and α-particles, the presented cross section is the sum of the (n,p) and (n,α) reactions, although apart from the first resonance the (n,α)-contribution is very small.

III. RESULTS

A. Cross section

Figure 3 shows the ^{36}Cl$(n,p)^{36}$S + ^{36}Cl$(n,\alpha)^{33}$P cross section in the neutron energy region from 500 eV to 250 keV.

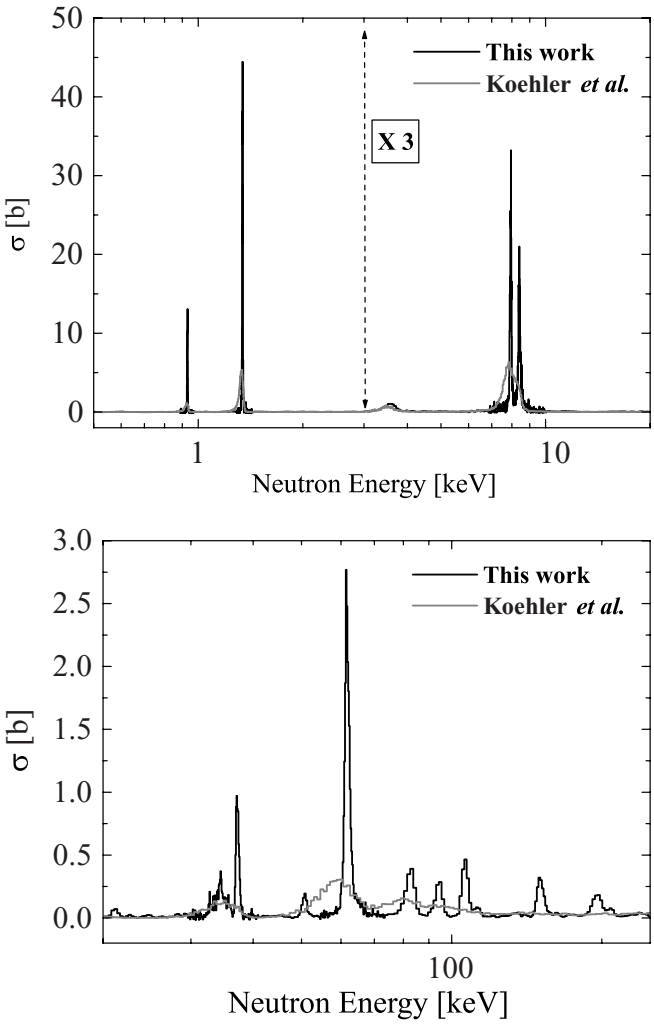

FIG. 3. ^{36}Cl$(n,p)^{36}$S plus ^{36}Cl$(n,\alpha)^{33}$P cross section determined in this work (black line) compared with the obtained cross section of Koehler *et al.* [2] (gray line).

A comparison with the obtained cross section in the measurement of Koehler *et al.* [2] is plotted in gray in the same Fig. 3. Due to the better energy resolution of the GELINA facility, many more resonances could be observed in this new measurement. The sources of uncertainties that influence the accuracy of the data can be divided in three categories: statistical uncertainties, overall normalization uncertainties and neutron energy dependent systematic uncertainties. Statistical uncertainties are depending on the cross sections of the measured reactions and, as a consequence, strongly vary with neutron energy. In the analysis, the statistical uncertainties for the ^{36}Cl and ^{10}B measurements have been taken into account. The overall normalization uncertainty of the data is determined by the uncertainties on the number of atoms in the ^{36}Cl and ^{10}B samples used. Apart from the uncertainty on the overall normalization of the data, there is the uncertainty on the correction for the time dependent background which consequently depends on the neutron energy. The data have been analyzed using AGS, a computer code for uncertainty propagation in time-of-flight cross section data which was

developed at IRMM [13]. It takes into account the different sources of uncertainty mentioned above and takes care of the error propagation during the different steps of the analysis, producing an experimental covariance matrix.

B. Resonance analysis

1. Fitting procedure

The determination of the resonance parameters is hampered by the broadening of the resonances due to the experimental resolution. This broadening is caused by several phenomena such as the promptness of the detector response and uncertainties on the flight path length, e.g., due to the moderation of the neutrons. The experimental broadening effects are represented by Gaussian functions and can be combined quadratically to find the total experimental broadening. So the resonance fitting procedure has to take into account the experimental broadening, which can be done in an elegant way by using the Voigt expression. A Voigt shape is a convolution of a Gauss and a Lorenz function, where the Lorenz expression represents the natural level width Γ and the experimental broadening can be regarded as the Gaussian contribution. The fit parameters of a Voigt function are the resonance energy E_{res}, the area of the resonance A_{res}, the Gaussian width Δ_G and the natural level width Γ. The Gaussian width Δ_G or broadening contribution can be calculated for each resonance and was taken fixed during the fit. For some resonances the Voigt fits are shown in Fig. 4. The experimental broadening Δ_G and the total fitted width $\Gamma_V = \sqrt{\Delta_G^2 + \Gamma^2}$ are plotted in Fig. 5 at the resonance energies. Only when the total width Γ_V is significantly bigger than the broadening width Δ_G, the fitted natural line width Γ can be regarded as the real natural line width of that resonance. From Fig. 5 it is clear that there are only a few resonances for which the total width is bigger than the experimental broadening. Only for these resonances the natural line width is calculated and listed in Table II together with the two other fit parameters, the peak position E_{res} and the resonance area A_{res}.

2. Spin assignments

s-wave neutrons interacting with the $I^\pi = 2^+$ ground state of ^{36}Cl can populate $J^\pi = \frac{3}{2}^+$ or $\frac{5}{2}^+$ states of the compound nucleus. For p-wave neutrons, states from $J^\pi = \frac{1}{2}^-$ through $\frac{7}{2}^-$ can be excited. As shown in the level scheme in Fig. 1, proton decay to the ground state ($J^\pi = 0^+$) of ^{36}S is allowed, but proton decay to the excited states of ^{36}S is energetically forbidden in the neutron energy range of this work. On the other hand, α-decay to the ground state ($J^\pi = \frac{1}{2}^+$) and to the first two excited states ($J^\pi = \frac{3}{2}^+$ and $J^\pi = \frac{5}{2}^+$) of ^{33}P is allowed. However, decay to the excited states of ^{33}P is less favored because of the smaller penetrability through the Coulomb barrier for the lower energetic α-particles. The smallest allowed angular momenta for the different decay possibilities are listed in Table III.

Whether the excited level in the compound nucleus is populated by an s-wave neutron or not, can be determined

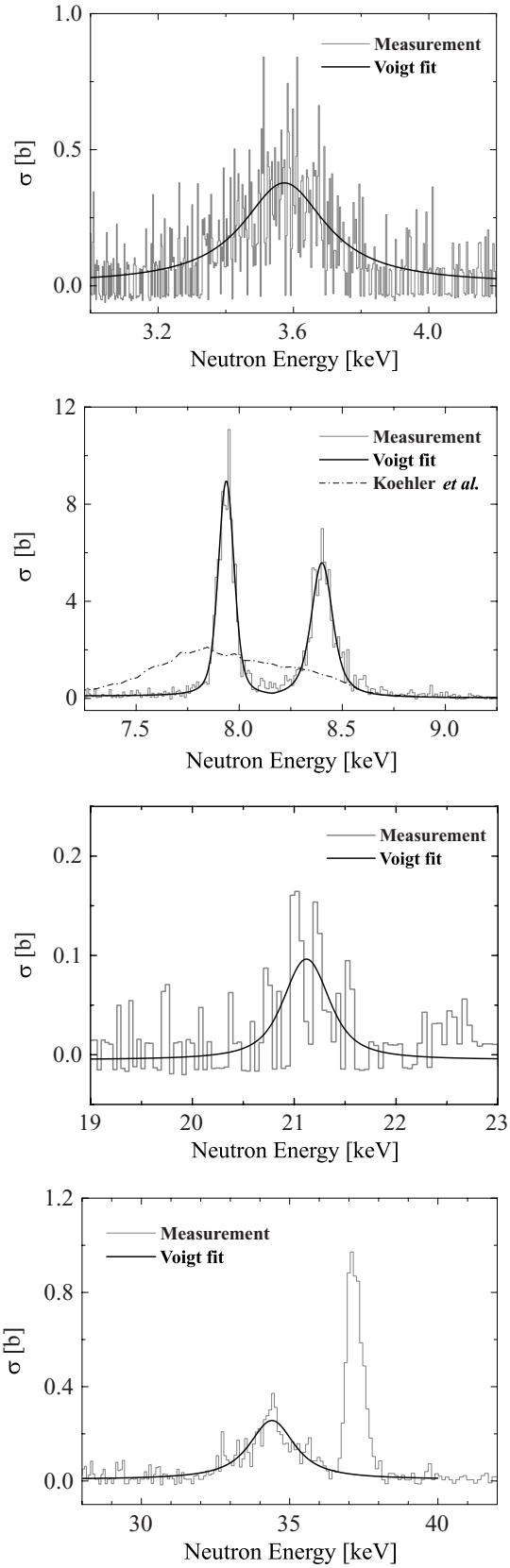

FIG. 4. Voigt fits to the ^{36}Cl$(n,p) + ^{36}$Cl(n,α) cross section data for some resonances. For the doublet at about 8 keV, the data obtained in this work are compared with the data of Koehler *et al.* [2], represented by the dashed line.

TABLE II. Resonance parameters obtained from the Voigt fits. The natural line width Γ is calculated only for these resonances for which the total fitted width is significantly bigger than the experimental broadening.

Energy [eV]	Area [b eV]	Γ [eV]
931 ± 1	57 ± 8	0.39 ± 0.08[a]
1341 ± 2	345 ± 30	
3570 ± 50	140 ± 50	300 ± 30
7937 ± 15	985 ± 80	
8400 ± 20	1000 ± 100	75 ± 25
21100 ± 300	50 ± 25	300 ± 250
34400 ± 200	500 ± 120	1600 ± 1000
37200 ± 100	625 ± 50	
50750 ± 200	255 ± 70	
61700 ± 200	4600 ± 400	
82700 ± 800	1500 ± 800	
94400 ± 800	1500 ± 600	
106500 ± 500	1600 ± 400	
112700 ± 1000	300 ± 200	
151000 ± 1500	1800 ± 600	
196000 ± 1500	2000 ± 1000	
208500 ± 3000	500 ± 300	

[a]This width is not significantly bigger than the experimental broadening. However, it could be calculated with the help of formula (8).

through the thermal cross section, as it is composed of the 1/v-tails of the different s-wave resonances, whereas the p-waves do not have a thermal contribution. The contribution of an s-wave resonance to the thermal cross section can be calculated with the following formula [14]:

$$\sigma(E_{\text{th}})[b] = 4.099 \times 10^6 \, \frac{g\Gamma_n^0\Gamma_p}{E_{\text{res}}^2}, \tag{5}$$

with g the statistical factor, Γ_n^0 the reduced neutron width in eV for an s-wave resonance, Γ_p in eV the proton width in the case of a (n,p) reaction and E_{res} the energy position of the resonance in eV. Making use of the following two formulas:

$$A_{\text{res}} = 2\left(\frac{\pi}{k_{\text{res}}}\right)^2 g\frac{\Gamma_n\Gamma_p}{\Gamma} \tag{6}$$

and

$$\Gamma_n(E_n) = \Gamma_n^0\sqrt{\frac{E_n}{1\,\text{eV}}}, \tag{7}$$

the contribution of an s-wave resonance to the thermal cross section can be rewritten as follows:

$$\sigma(E_{\text{th}})[b] = \frac{1}{2\pi\sqrt{E_{\text{th}}}}\frac{\Gamma_{\text{res}}A_{\text{res}}}{E_{\text{res}}^{3/2}}, \tag{8}$$

with Γ_{res}, E_{res}, and E_{th} in eV and A_{res} in b eV.

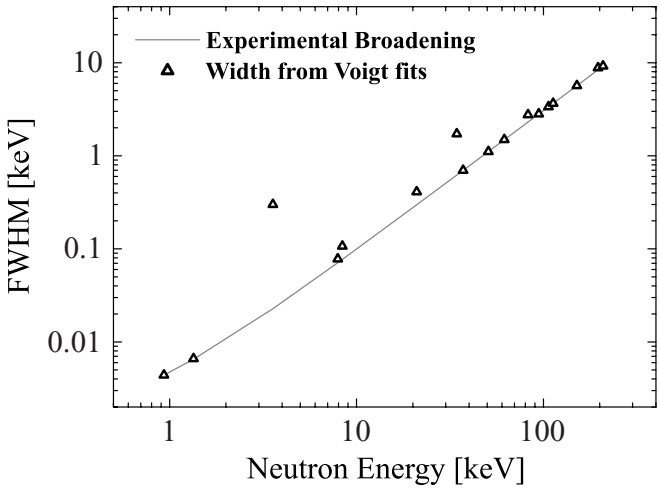

FIG. 5. The total width obtained from the Voigt fits for each observed resonance (triangles) compared with the calculated experimental broadening (gray line).

TABLE III. Smallest allowed angular momenta of the emitted particles from the formed compound nucleus ^{37}Cl in the case of impinging s- or p-wave neutrons.

Final state	J^π ^{37}Cl compound nucleus					
	s-wave		p-wave			
	$\frac{3}{2}^+$	$\frac{5}{2}^+$	$\frac{1}{2}^-$	$\frac{3}{2}^-$	$\frac{5}{2}^-$	$\frac{7}{2}^-$
^{36}S: 0^+ (p_0)	2	2	1	1	3	3
^{33}P: $\frac{1}{2}^+$ (α_0)	2	2	1	1	3	3
^{33}P: $\frac{3}{2}^+$ (α_1)	0	2	1	1	1	3
^{33}P: $\frac{5}{2}^+$ (α_2)	2	0	3	1	1	1

This contribution is calculated for the resonances for which the natural line width is listed in Table II—with the exception of the first resonance. If this calculated value is higher than the measured thermal cross section, the resonance is taken as a p-wave. Only the resonance around 21 keV stays far below the measured thermal cross section of (47 ± 2) mb [10] and is taken to be s-wave. The thermal contribution for the other resonances is much higher than 47 mb, so they are expected to be p-wave.

It is mentioned in this subsection that only the first resonance has a significant α-contribution. This means that this resonance must be responsible for the measured thermal α-cross section of 590 ± 70 μb [10]. As the thermal cross section is composed of the 1/v-tails of the s-wave resonances, it can be concluded that the first resonance at 931 eV has to be an s-wave resonance. With this knowledge and making use of formula (8), the total width Γ_{res} of the first resonance can be calculated and is found to be (0.39 ± 0.08) eV.

3. Determination of the partial level widths

Apart from the measurement of Koehler *et al.* [2], there are only two measurements reported from which information can be derived about the resonances. The first one is a ^{36}S$(p,\gamma)^{37}$Cl measurement by Nooren *et al.* [15]. They observed three resonances corresponding to a neutron energy between 0 and 8 keV in the laboratory system, for which the resonance strength $\omega_\gamma = (2J+1)\frac{\Gamma_\gamma\Gamma_p}{\Gamma}$ is reported. Comparison with the data obtained in this work indicates that they

TABLE IV. Comparison of the resonance parameters obtained in this work with the parameters reported by Koehler *et al*. [2] and Gledenov *et al*. [1].

	Energy [eV]	ℓ	Γ [eV]	ω_p [eV]
This work	931 ± 1	0	0.39 ± 0.08	0.013 ± 0.002
	3570 ± 50	1	300 ± 30	0.122 ± 0.044
	8400 ± 20	1	75 ± 25	2.05 ± 0.21
	21100 ± 300	0	300 ± 250	0.26 ± 0.13
	34400 ± 200	1	1600 ± 1000	4.21 ± 1.01
Koehler *et al*. [2]	928 ± 1.3	0	$0.84\ ^{+2.4}_{-0.51}$	0.0063 ± 0.0008
	3510 ± 40	1	$280\ ^{+140}_{-80}$	0.096 ± 0.019
	8300 ± 45	0	$40\ ^{+80}_{-31}$	0.95 ± 0.19
	20495 ± 500	0	$1140\ ^{+2660}_{-1040}$	0.11 ± 0.05
	34675 ± 540	1	$2090\ ^{+1160}_{-790}$	6.4 ± 1.5
Gledenov *et al*. [1]	3500 ± 300			0.08 ± 0.03
	8200 ± 900			1.7 ± 0.3

did not resolve the 0.93 keV and 1.34 keV doublet nor the 7.94 keV and 8.40 keV doublet. The second measurement is a $^{36}S(p,\gamma)^{37}Cl$ measurement by Vodin *et al*. [16]. They reported resonance strengths ω_γ for the resonances observed in their measurement. Once again they did not resolve the doublets around 1 keV and 8 keV. The resonance strengths listed by Vodin *et al*. [16] for the three resonances observed by Nooren *et al*. [15] are comparable. Therefore, it is assumed that the resonance strengths reported by Vodin *et al*. [16] may be used for the determination of the partial level widths for the five resonances of this work for which the natural line width could be calculated (see Table II).

For these resonances, three equations are available:

$$\Gamma = \Gamma_n + \Gamma_\gamma + \Gamma_p,$$
$$\omega_p = g\frac{\Gamma_n\Gamma_p}{\Gamma} = \frac{2J+1}{10}\frac{\Gamma_n\Gamma_p}{\Gamma},$$
$$\omega_\gamma = (2J+1)\frac{\Gamma_\gamma\Gamma_p}{\Gamma}.$$

Combining them leads to the following solutions for the unknown Γ_γ, Γ_n and Γ_p:

$$\Gamma_\gamma = \frac{\Gamma \pm \sqrt{\Gamma^2 - \frac{4\Gamma}{2J+1}\left(10\omega_p + \omega_\gamma\right)}}{2\left(10\frac{\omega_p}{\omega_\gamma}+1\right)},$$

$$\Gamma_n = 10\frac{\omega_p}{\omega_\gamma}\Gamma_\gamma, \tag{9}$$

$$\Gamma_p = \frac{\omega_\gamma\Gamma}{(2J+1)\Gamma_\gamma}.$$

For the doublet around 8 keV, which was not resolved in the data of Vodin *et al*. [16], the reported ω_γ is split up in two equal parts for each resonance. So, for each J-value, two sets of partial widths are possible. Based on the systematics for excited levels in this mass region, the positive sign of the square root in Eq. (10) may for most of the cases be ruled out because Γ_γ will be too high. For the moment J is not determined unambiguously, therefore no partial level widths are listed. However, by trying all the possibilities for J and by taking the negative square root, it turned out that in every case Γ_p almost equals Γ. In addition, by increasing J, Γ_p approaches Γ more and more. This means that

$$\omega_p = g\frac{\Gamma_n\Gamma_p}{\Gamma} \sim g\Gamma_n, \tag{10}$$

or the resonance strength (or the area) of the resonance completely determines Γ_n.

If J can be determined through additional measurements leading to the same ^{37}Cl compound nucleus, the partial widths can be deduced from the set of equations listed above. Then these deduced partial widths and accompanying spin may be used as input parameters in resonance shape analysis (RSA) programs to accurately determine the total and partial level widths of the states in the compound nucleus.

4. Discussion

Firstly, by measuring the $^{36}Cl(n,p)+^{36}Cl(n,\alpha)$ reactions as a function of the neutron energy 17 resonances are observed in the energy region up to approximately 250 keV, which is much more than the eight observed before by Koehler *et al*. [2]. This is due to the better energy resolution at GELINA by which resonances could be resolved from each other. This is nicely shown in Figs. 3 and 4.

Secondly, in Table IV the spin assignments, level widths and resonance strengths for each of the five resonances obtained in this work are compared with the ones obtained in the work of Koehler *et al*. [2] and Gledenov *et al*. [1]. The table shows that the energy precision obtained in this work is better than before. Furthermore, the obtained resonance parameters are in excellent agreement with the data of Koehler *et al*. [2] and Gledenov *et al*. [1]. Only the spin assignment for the resonance at 8.4 keV is different from the one derived by Koehler *et al*. [2]. However, their resonance strength and level width Γ are about two times smaller than those obtained in this work. Furthermore, the thermal contribution in the case of an s-wave resonance is proportional to both parameters [see formula (8)], and by taking the parameters listed by Koehler *et al*. [2] the

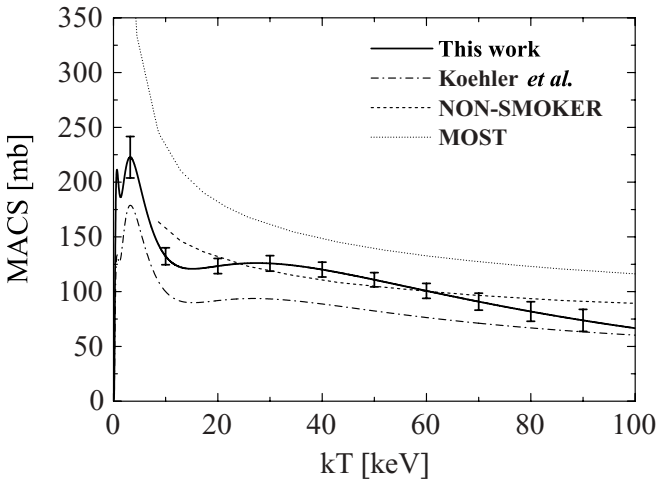

FIG. 6. The ^{36}Cl$(n,p)^{36}$S + ^{36}Cl$(n,\alpha)^{33}$P MACS values represented by the full line obtained by numerical integration of the obtained cross section data. A comparison is made with the data of Koehler *et al*. [2] (dashed dotted line) and with theoretical values.

contribution stays below the thermal value, indeed leading to an s-wave. Nevertheless, in the cross section data of Koehler *et al*. [2] it was difficult to resolve the doublet around 8 keV. Therefore it can be possible that the distribution of the areas and the Γ's over the two resonances is incorrect in the work of Koehler *et al*. [2], explaining the difference in spin assignment.

Finally, it can be concluded that the resonance parameters obtained in this work are in agreement with the previous measurements. But the accuracy obtained in this work is better leading to more reliable resonance parameters and MACS values.

IV. ASTROPHYSICAL IMPLICATIONS

A. Determination of the MACS

The MACS values shown in Fig. 6 are calculated by numerical integration of the obtained cross section. They are compared with the values reported by Koehler *et al*. [2] and a reasonable agreement is found between both. This is not surprising since the poorer resolution in the experiment of Koehler *et al*. [2] does not affect the MACS computation. The calculated MACS values are compared with theoretical values of MOST [17] and NON-SMOKER [18]. A good agreement with the NON-SMOKER calculations can be observed. This comparison might however not be meaningful, since the level density in the theoretical calculations is probably too low for reliable statistical model calculations for light nuclei.

B. Origin of ^{36}S

As quoted in the introduction, ^{36}S is believed to be synthesized mainly during the s-process, in particular the weak component of the s-process in massive stars [19]. An additional, but smaller contribution may come from He-shell burning in low mass AGB stars during the main s-process [20,21]. The suggestion of an s-process origin for ^{36}S is supported by the detection of ^{36}S bearing molecules in the interstellar medium where the ^{34}S/^{36}S ratio of 115 ± 17 [22] was far below the solar ratio of 288 [23]. This difference indicated that ^{36}S must be produced in a process different from that of the other sulfur isotopes.

To verify this s-process hypothesis, nucleosynthesis network calculations in the mass region between $28 \leqslant A \leqslant 42$ are necessary. This s-process network is depicted in Fig. 7. It can be seen that the measured ^{36}Cl$(n,p)^{36}$S reaction influences the ^{36}S abundance in a direct way. However, the ^{34}S(n,γ) reaction turns out to be the most important reaction towards ^{36}S [24,25]. The experimentally determined ^{34}S(n,γ) cross section is very low [26], causing a bottleneck effect for the reaction flow from ^{34}S to ^{36}S. The main effect of the small ^{34}S cross section is a significant suppression of the mass flow from the abundant seed nuclei ^{28}Si and ^{32}S. Consequently, the rarer isotope ^{35}Cl is replacing ^{34}S as important seed for the ^{36}S production.

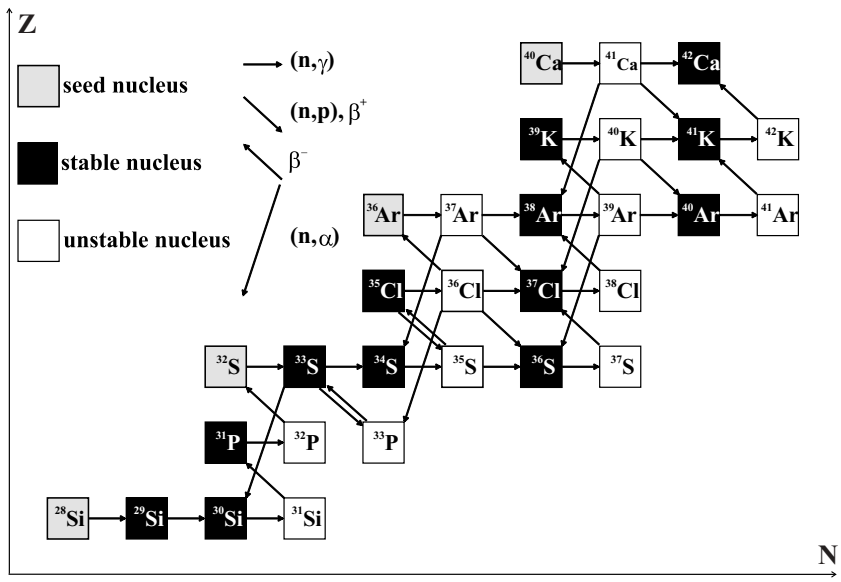

FIG. 7. s-process synthesis path in the mass region $28 \leqslant A \leqslant 42$.

The new ^{36}Cl$(n,p)^{36}$S MACS values are used in stellar model calculations by Gallino *et al*. at the university of Torino. They concluded that the galactic contribution from the main s-process, occurring in AGB stars during the convective He pulses, to solar ^{36}S is very minor. On the other hand, the weak s-process, occurring in massive stars during convective He-core burning followed by convective C-shell burning, can be ascribed to account for almost the entire production of solar ^{36}S. Still, some additional ^{36}S contribution is needed to explain the total solar ^{36}S abundance. At present, it is assumed that improved network calculations and the inclusion of presupernova and explosive nucleosynthesis may account for this missing solar ^{36}S contribution [27,28]. The calculations to confirm these assumptions are in full progress.

V. CONCLUSION

In the present work the ^{36}Cl$(n,p)^{36}$S+^{36}Cl$(n,\alpha)^{33}$P reaction cross section has been determined from 500 eV up to approximately 250 keV. Seventeen resonances were identified with a high accuracy. For each of them the resonance position and strength have been determined. Additionally, for five resonances the spin and total level width could be calculated. They are in good agreement with previous data, but the achieved accuracy is better. The calculated MACS values are used in stellar model calculations to trace the origin of ^{36}S. The new MACS values reveal that the weak component of the s-process occurring in massive stars accounts for almost the entire production of solar ^{36}S.

[1] Y. M. Gledenov, Y. P. Popov, and V. I. Salatsky, Z. Phys. A **322**, 685 (1985).
[2] P. E. Koehler, S. M. Graff, H. A. O'Brien, Y. M. Gledenov, and Y. P. Popov, Phys. Rev. C **47**, 2107 (1993).
[3] R. Bieber, C. Wagemans, J. Heyse, N. Balcaen, R. Bartélémy, and J. Van Gils, Proceedings of the 9th International Symposium on Capture Gamma Ray Spectroscopy and Related Topics, Budapest, Hungary, 1997, p. 443.
[4] C. Wagemans, G. Goeminne, L. De Smet, and J. Wagemans, Proceedings of the 17th Divisional Conference on Nuclear Physics in Astrophysics (NPDC17), ATOMKI, Debrecen, Hungary, 2002.
[5] G. Goeminne, Ph.D. thesis, Vakgroep Subatomaire en Stralingsfysica, Universiteit Gent (2001).
[6] A. Bensussan and J. M. Salome, Nucl. Instrum. Methods **155**, 11 (1978).
[7] W. Mondelaers and P. Schillebeeckx, Notiziario neutroni e luce di sincrotrone **11.2**, 19 (July 2006).
[8] O. Bunemann, T. E. Cranshaw, and J. A. Harvey, Can. J. Res. **27 A**, 191 (1949).
[9] J. Gonzalez, C. Bastian, S. de Jonge, and K. Hofmans, Modular MultiParameter Multiplexer MMPM. Hardware Description and User Guide, 1997, IRMM Internal Report GE/R/INF/06/97.
[10] C. Wagemans, R. Bieber, and P. Geltenbort, Phys. Rev. C **54**, 389 (1996).
[11] R. Eykens, A. Goetz, A. Lamberty, J. Van Gestel, J. Pauwels, C. Wagemans, S. Druyts, and P. D'hondt, Nucl. Instrum. Methods Phys. Res. A **303**, 152 (1991).
[12] http://www-nds.iaea.org/endf
[13] C. Bastian, Proceedings of the International Conference on Neutron Research and Industry, Crete, Greece, 1996.
[14] S. F. Mughabghab, *Atlas of Neutron Resonances*, 5th ed. (Elsevier, Amsterdam, 2006).
[15] G. J. L. Nooren and C. van der Leun, Nucl. Phys. **A423**, 197 (1984).
[16] A. N. Vodin, A. S. Kachan, V. M. Mishchenko, and R. P. Slabospitsky, Bull. Russ. Acad. Sci. Phys. **60**, 1821 (1996).
[17] S. Goriely, http://www-astro.ulb.ac.be/Html/ncap.html.
[18] T. Rauscher, http://nucastro.org/reaclib.html.
[19] H. Beer and R.-D. Penzhorn, Astron. Astrophys. **174**, 323 (1987).
[20] O. Straniero, R. Gallino, M. Busso, A. Chieffi, C. M. Raiteri, and M. Limongi, Astrophys. J. Lett. **440**, L85 (1995).
[21] R. Gallino, C. Arlandini, M. Busso, M. Lugaro, C. Travaglio, O. Straniero, A. Chieffi, and M. Limongi, Astrophys. J. **497**, 388 (1998).
[22] R. Mauersberger, C. Henkel, N. Langer, and Y.-N. Chin, Astron. Astrophys. Lett. **313**, L1 (1996).
[23] T. Ding, S. Valkiers, H. Kipphardt *et al*., Geochim. Cosmochim. Acta **54**, 2433 (2001).
[24] H. Schatz, S. Jaag, G. Linker, R. Steininger, F. Käppeler, P. E. Koehler, S. M. Graff, and M. Wiescher, Phys. Rev. C **51**, 379 (1995).
[25] W. M. Howard, W. D. Arnett, D. D. Clayton, and S. E. Woosley, Astrophys. J. **175**, 201 (1972).
[26] R. Reifarth, K. Schwarz, and F. Käppeler, Astrophys. J. **528**, 573 (2000).
[27] R. Gallino (private communication, 2005).
[28] R. Mauersberger, U. Ott, C. Henkel, J. Cernicharo, and R. Gallino, Astron. Astrophys. **426**, 219 (2004).